nature COMMUNICATIONS

ARTICLE

DOI: 10.1038/s41467-017-02250-4 OPEN

Solution-phase synthesis of Al_{13}^- using a dendrimer template

Tetsuya Kambe[1,2], Naoki Haruta[2], Takane Imaoka[1,2,3] & Kimihisa Yamamoto[1,2]

Superatoms, clusters that mimic the properties of elements different to those of which they are composed, have the potential to serve as building blocks for unprecedented materials with tunable properties. The development of a method for the solution-phase synthesis of superatoms would be an indispensable achievement for the future progress of this research field. Here we report the fabrication of aluminum clusters in solution using a dendrimer template, producing Al_{13}^-, which is the most well-known superatom. The Al_{13}^- cluster is identified using mass spectrometry and scanning transmission electron microscopy, and X-ray photoelectron spectroscopy is used to measure the binding energies. The superatomic stability of Al_{13}^- is demonstrated by evaluating its tendency toward oxidation. In addition, the synthesis of Al_{13}^- in solution enables electrochemical measurements, the results of which suggest oxidation of Al_{13}^-. This solution-phase synthesis of Al_{13}^- superatoms has a significant role for the experimental development of cluster science.

[1] Laboratory for Chemistry and Life Science, Institute of Innovative Research, Tokyo Institute of Technology, Yokohama 226-8503, Japan [2] ERATO-JST, Institute of Innovative Research, Tokyo Institute of Technology, Yokohama 226-8503, Japan [3] PRESTO-JST, Institute of Innovative Research, Tokyo Institute of Technology, Yokohama 226-8503, Japan Correspondence and requests for materials should be addressed to K.Y. (email: yamamoto@res.titech.ac.jp)

Superatoms, clusters that exhibit properties similar to those of elements different to those of which they are composed, have the potential to serve as building blocks for unprecedented materials with tunable properties. Studies on superatoms have been mainly theoretical and have been supported by mass detection in the gas phase under high-vacuum conditions[1,2]. With regard to further progress in this research field, achieving a solution-phase synthetic method for superatoms is important. The approach using noble metals Au, Ag, and Cu produces ligand-protected clusters, and although they have produced cluster crystals[3,4], these are thermodynamically stable magic clusters. Therefore, a more advanced synthetic strategy is required.

Experimental studies on superatoms started with the synthesis of vaporized sodium and aluminum clusters[5,6], and have attracted wide attention since the discovery of the Al_{13} halogen-like superatom by Khanna et al[7]. This was followed by the synthesis of Al_7, As_7, and KO_3[8–10]. Superatom properties can be estimated using a simple theory referred to as the Jellium model[11] that defines superatomic orbitals (e.g., 1S, 1P, 1D, 2S, 1F, 2P) in a highly symmetric cluster. For example, the Al_{13} cluster has 39 valence electrons and exhibits a halogenic nature based on its superatomic orbitals ($1S^2$, $1P^6$, $1D^{10}$, $2S^2$, $1F^{14}$, $2P^5$), resulting in a reactivity with I^- and the high stability of the mono anionic species Al_{13}^-[7,12].

The aluminum clusters with anionic or cationic states have been extensively studied and confirmed by gas-phase synthesis and quantum chemical calculations[13–15]. Such a study also revealed photoelectron spectroscopy about the energy levels of the valence electrons using laser light, and the superatom character of Al_{13}^- containing an extraordinary stability against oxidation[16–18]. On the other hand, the solution-phase synthesis has advantages because the synthesis is scalable without any special apparatus. Although poly(vinylpyrrolidone) or tetrahydrofuran (THF) units have been reported to theoretically stabilize the Al_{13} cluster[19,20], the solution-phase synthesis of Al_{13}^- has not yet been achieved, but is expected[21].

Specially designed dendrimers are one of the effective tools for the synthesis of superatoms because metal units can be set inside the structure and are protected by the shell-effect of the dendrons[22–26]. Dendritic poly-phenylazomethines[25,27–32] (DPAs) have been developed that can provide various size-controlled metal clusters[24]. From these features, the DPAs have a potential to be a template for superatom synthesis though the capsuling dendrimer has a risk to prevent some features from the superatoms.

Here, we use this method to synthesize the aluminum clusters including Al_{13}^-, which is the best-known superatom. This approach enables core-level X-ray photoelectron spectroscopy (XPS) and electrochemical measurements, which are not compatible with the gas-phase synthetic approaches. By investigating a series of aluminum clusters, the superatomic nature of Al_{13}^- in solution is confirmed.

Results

Fabrication of aluminum clusters using DPAG4. The preparation method is illustrated in Fig. 1a. The number of Al atoms in the clusters was controlled using the stepwise assembly feature of the DPAs. The fourth-generation DPA dendrimer (DPAG4) and that with a pyridine core (pyDPAG4) were used (Supplementary Fig. 1). The assembly of $AlCl_3$ was confirmed by UV–Vis titration; the absorption change in a THF solution of the DPAG4 or pyDPAG4 during the addition of $AlCl_3$ indicated complexation behavior between the imine site and $AlCl_3$ in a radial fashion, and a multi-step shift of the isosbestic point provided evidence that the targeted amounts of the $AlCl_3$ were coordinated in the DPAs[24]. The DPAG4 enabled the controlled assembly of 4, 12, 28, and 60 units of $AlCl_3$ (Supplementary Fig. 2). In contrast, the pyDPAG4, which has a pyridine core that can coordinate one additional metal salt, enabled the assembly of 13 units of $AlCl_3$ in the dendritic capsule. Supplementary Figure 3 shows assembly of $AlCl_3$ from 0 to 61 equivalents. The obvious change in the isosbestic point at 13 equivalents demonstrates preparation of $13AlCl_3$–pyDPAG4 in solution. The $AlCl_3$ units positioned in the DPAs were reduced into clusters by a benzophenone ketyl radical prepared using sodium metal in THF. The fabricated aluminum clusters were then subjected to various experiments. The aluminum clusters with 14 atoms were prepared using the DPAG4. Even though the branched structure of the DPAG4 was not the best for 14 atom clusters, the enough ability to fabricate the cluster as the major product with small deviation was already reported in our previous work[29].

The fabricated cluster was protected by the dendrimer shell; however, the superatomic Al_{13}^- could be detected using negative-mode matrix-assisted laser desorption/ionization (MALDI) mass spectrometry at $m/z = 350.9$ via dissociation from the DPA template during the laser desorption process. This peak was overlapped by a fragment of the pyDPAG4, but the formation of Al_{13}^- in solution was still confirmed (Fig. 1b). Al_{13}^- was specifically observed when the $13AlCl_3$-pyDPAG4 complex was reduced, whereas it was not detected for $12AlCl_3$-pyDPAG4 and $14AlCl_3$-pyDPAG4 (Supplementary Fig. 4). In addition, the Al_{13}^- cluster was detected using high-angle annular dark-field scanning transmission electron microscopy (HAADF-STEM). The observed cluster sizes were measured to be 1.0 ± 0.1 nm (Fig. 1c, d). The cluster sizes were reasonable considering the calculated diameter of Al_{13}^- (0.95 nm, see Methods). These results confirm that the Al_{13}^- superatom exists in solution.

Electronic state. The oxidation states of the clusters were estimated from XPS Al 2p spectra. The XPS samples were prepared on glassy carbon substrates by repetitive drop-casting. The spectra and binding energies (BEs) of the aluminum clusters which were synthesized using 4, 12, 13, 28, and 60 $AlCl_3$ at the DPAs are summarized in Fig. 2a, b, respectively. All the aluminum clusters possessed BEs equal or lower than that of bulk aluminum, thereby indicating the presence of reduced clusters. In addition, the BE for $n = 13$ cluster seems to be different from the BEs for $n = 4$, 12, and 28 atomic clusters (Fig. 2b). Although the XPS spectra generally reflect the surface state of materials, it is not applied to these aluminum clusters because they have lower than or equal to 60 atoms with the diameters of about 1 nm. Considering that the photoelectrons can escape from about a 1–4 nm thick material[33], almost all atoms in the clusters were analyzed.

To interpret these XPS results in a theoretical manner, population analyses for aluminum clusters including Al_{13}^- were performed (Supplementary Fig. 5). The employed structures were based on the literatures[34,35]. To estimate the charge distribution effect on the 2*p* binding energies, we have calculated the 2*p* orbital levels. Although core-hole relaxation in the final state has not been taken into account, simple correlation between core levels and binding energies has been reported[36]. In the case of Al_{13}^-, the 2*p* levels of the inner atom are apart from those of surface atoms (Supplementary Fig. 6). This difference offers possibility of two peaks in the XPS spectrum. However, only one broad peak was detected in our experiments. The observed peak could be ascribed to 12 surface atoms or the mixture of 12 surface atoms and an inner atom. Also, in the cases of anionic clusters in other sizes, the non-uniform charge distributions yield different 2*p* levels, as shown in Supplementary Fig. 7a. However, all the 2*p* levels are

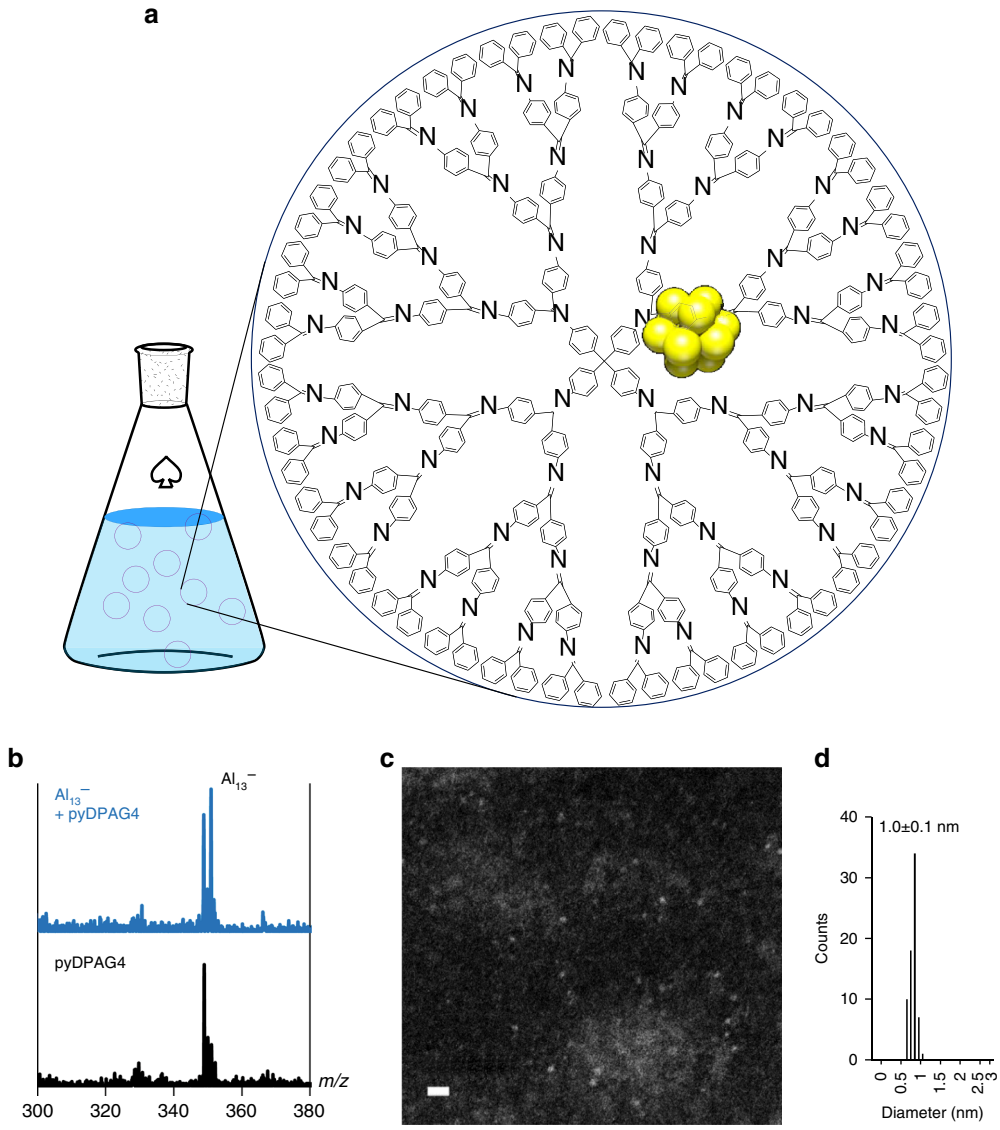

Fig. 1 Fabrication of Al_{13}^- using the dendrimer template. **a** Illustration of dendritic poly-phenylazomethines including an aluminum cluster in the solution state. **b** Negative-mode matrix-assisted laser desorption/ionization mass spectra of Al_{13}^- and blank. 1,8,9-Trihydroxyanthracene was used as the matrix. **c** A high-angle annular dark-field scanning transmission electron microscopy image of Al_{13}^- on a TEM grid covered with a thin carbon film (scale bar: 5 nm). **d** Histogram of the observed particle sizes in the STEM sample

close and overlap to be one broad peak. The size dependence of the 2*p* levels of anionic clusters is consistent with our experimental results. This is in contrast to the neutral clusters (Supplementary Fig. 7b).

These shift of binding energy in the XPS measurements and calculated energy levels could be considered by the influence of the negative charges. The charges per atom were simply calculated based on the assumption that the anionic charges are fully delocalized in the aluminum clusters (Supplementary Fig. 8). The anionic charges per atom increased as the number of atoms decreased. This tendency was in agreement with the observed BEs. Therefore, these BEs are assignable to monovalent or more than divalent anionic states.

Stability. The reactivity of the aluminum clusters with oxygen was evaluated by monitoring the change in the XPS Al 2*p* peaks. The samples deposited on the substrates with the DPAs were exposed to air and subjected to Ar sputtering (2 kV, 2 min) to remove any surface impurities before the measurement. The results are shown in Fig. 3. The peaks corresponding to the oxidized species from Al_{12} and Al_{14} clusters increased within several tens of hours, whereas the peak for Al_{13}^- maintained its position. This result demonstrates the specific stability of the Al_{13}^- clusters toward oxygen and is consistent with the superatomic nature observed in the gas phase[18]. The clusters observed within the DPAs were deposited with ketyl radical salts; however, they did not affect the stability because the radical anions were quickly oxidized in air within several minutes (Supplementary Fig. 9). The extraordinary stability of Al_{13}^- was well theoretically investigated in previous reports[37–39]. In addition, inclusive studies of aluminum clusters were also reported with their local and global minima[34,40,41]. They fully supported our result.

Electrochemical oxidation. The oxidation processes of the prepared aluminum clusters in the DPAs were investigated by potentiodynamic electrochemical measurements in THF

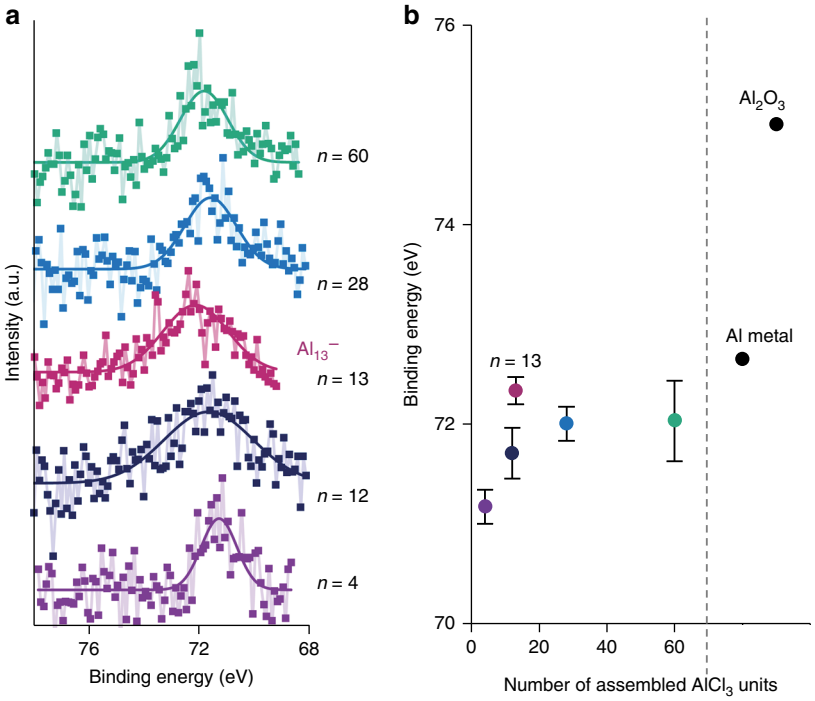

Fig. 2 X-ray photoelectron spectroscopy results of the aluminum clusters. **a** XPS spectra and **b** binding energies of the Al_n cluster samples, aluminum metal and Al_2O_3. n (= 4, 12, 13, 28, and 60) is the number of assembled $AlCl_3$ units in the DPAs. Error bars in **b** stand for the standard deviation of the mean of three independent experiments

solutions containing the sodium benzophenone ketyl radical (Fig. 4). To unify the materials in the cell, DPAG4 was used for all the aluminum clusters. All steps of the measurements were conducted under an Ar atmosphere. The open circuit potentials of the samples were approximately −1.7 V vs. Ag/Ag^+. The potential was then swept to higher values. The Al_{13}^- cluster exhibited a shoulder-like peak (i) at −0.97 V and a second oxidation peak (ii) at −0.73 V (Fig. 4b, black arrows). The cyclic voltammogram of $AlCl_3$ measured in THF showed a reduction wave of $AlCl_3$ below −1.0 V and an increase of the oxidation current from −0.6 V (Supplementary Fig. 10). Considering these results, the first oxidation step observed in the Al_{13}^- sample could be assigned to oxidation from Al_{13}^- to Al_{13}^0. The oxidation current of Al_{13}^- was maintained after the process, which suggests that the oxidized clusters were then re-reduced by the benzophenone ketyl radicals in the cell. This one electron oxidation of Al_{13}^- suggested tuning of the electronic state by the applied electronic potential in solution. In contrast, both Al_{12} and Al_{14} clusters exhibited different phenomena, and only an intense oxidation peak that corresponded to the second oxidation process was observed for Al_{13}^- (Fig. 4a, c). As their oxidation potentials were nearly the same, these intense peaks are considered to be derived from the oxidation of the aggregated aluminum clusters on the surface of the working electrode and organic materials arising from the DPAG4.

Discussion

The fabricated clusters were protected by the DPA template. It is useful for synthesis of clusters in solution[27-29], however, the features have possibility to be different from the inherent character. Considering the isolation of clusters from the DPAs, stability of the clusters is a crucial factor.

In conclusion, aluminum clusters, including the superatomic Al_{13}^- species, were fabricated in solution by utilizing the controlled metal assembly of DPA templates. To the best of our knowledge, this is the first example of the synthesis of the benchmark Al_{13}^- superatom in solution. The Al_{13}^- cluster was identified by mass spectrometry and STEM measurements. In addition, specific features of the Al_{13}^- in the XPS, oxidation reaction and electrochemical measurement demonstrated its successful synthesis in solution. The oxidation states of the aluminum clusters were determined from BEs measured in XPS Al 2*p* spectra. The stability and reactivity of Al_{13}^- were compared with those of other aluminum clusters. The particularly high stability of Al_{13}^- was demonstrated by air exposure and through theoretical calculations. In addition, the aluminum clusters in solution exhibited redox behavior derived from Al_{13}^-/Al_{13} in DPAG4. The solution-phase synthesis of Al_{13}^- superatoms has a significant role for the experimental development of cluster science.

Methods

Materials. pyDPAG4 and DPAG4 were synthesized by a convergent method. The fourth-generation phenylazomethine dendrons were connected to the core molecules. The detailed procedures are described in previous reports[42,43]. $AlCl_3$ (ultra dry) was purchased from Alfa Aesar, a Johnson Matthey Company. Dehydrated THF (stabilizer-free) was obtained from Kanto Chemicals. Sodium metal, benzophenone and tetrabutylammonium hexafluorophosphate were obtained from Wako Pure Chemical Industries, Ltd. and TCI Co., Ltd.

Assembly of $AlCl_3$ in pyDPAG4. The experiment was conducted in an N_2-filled glove box. A THF solution of $AlCl_3$ (2.60 mM) and pyDPAG4 (4.01 μM) was prepared. An appropriate equivalent of $AlCl_3$ solution was then added to the DPAG4 solution. Complexation between $AlCl_3$ and DPAG4 was monitored using UV–Vis spectroscopy.

Assembly of $AlCl_3$ in DPAG4. The experimental procedure was conducted in the same way as that with pyDPAG4. The concentrations of $AlCl_3$/THF and DPAG4/THF were 5.41 mM and 5.06 μM, respectively.

Fabrication of aluminum clusters. pyDPAG4 was used for the Al_{13}^- cluster, and DPAG4 was used for the Al_4, Al_{12}, Al_{14}, Al_{28}, and Al_{60} clusters. The inferior number (n) of Al_n reflects the added equivalent of the $AlCl_3$ in the DPAs.

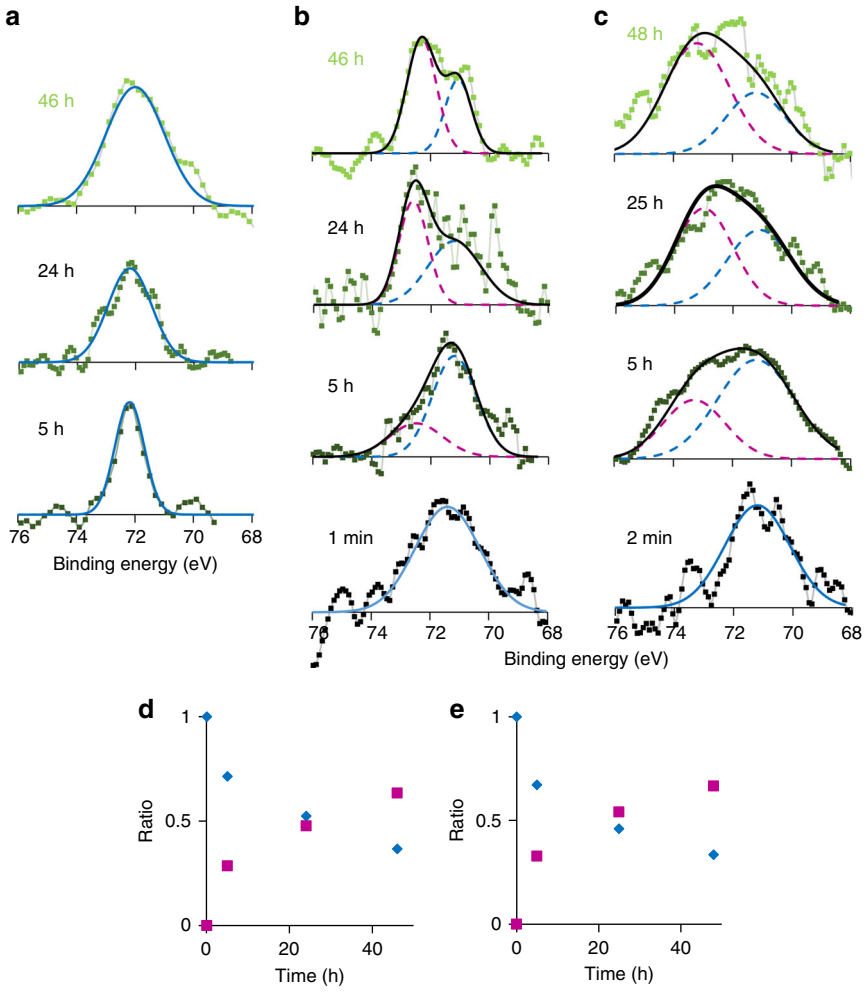

Fig. 3 Change in the XPS Al 2*p* peaks upon air exposure. The graphs show the spectral change for the Al_n clusters. **a** $n = 13$, **b** $n = 12$, and **c** $n = 14$. The exposure times were 1–2 min, 5 h, 24–25 h, and 46–48 h. The vertical axes are normalized intensity. The spectra for Al_{12} and Al_{14} samples could be fitted by two peaks derived from the initial reduction peak (blue dashed line) and oxidation peak (red dashed line). Ratio of the oxidized (red squares) to the as-prepared (blue diamonds) peaks for **d** Al_{12} and **e** Al_{14} samples

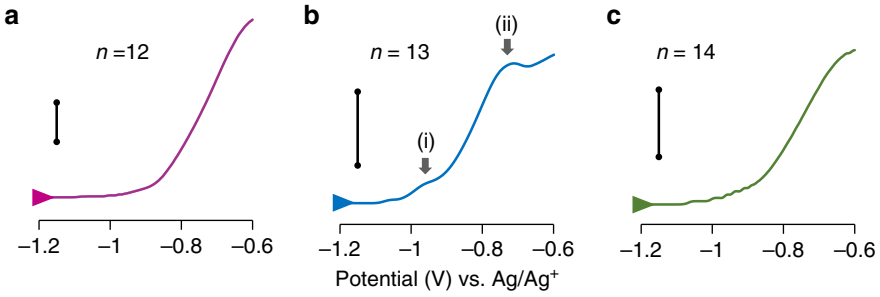

Fig. 4 Oxidation waves of the fabricated anionic aluminum cluster samples. They correspond to Al_n clusters. **a** $n = 12$ (6 μM), **b** $n = 13$ (4 μM), and **c** $n = 14$ (4 μM) in THF. The potential sweep was started from −1.7 or −1.8 V (open circuit potentials) at the scan speed of 0.025 V/s. Black bars indicate 10 μA in **a** and **c**, and 5 μA in **b**. $NaPF_6$ was used as an electrolyte (0.05 M)

Dendrimer solutions in THF (3–8 μM) were prepared in an Ar-filled glove box. The required equivalents of $AlCl_3$ in THF were added to each dendrimer solution to prepare the $AlCl_3$-complex dendrimer. The benzophenone ketyl radical was prepared by the addition of an excess amount of sodium metal into the solution of benzophenone in THF (0.3 M). The THF solution of benzophenone ketyl radicals (1 mL) was added to the prepared $AlCl_3$-complex solution (1 mL) to fabricate aluminum clusters at the DPAs. Samples for STEM measurements were prepared by the use of 60 equivalents of benzophenone to $AlCl_3$ for reduction.

Characterization. UV–Vis spectra were recorded at 20 °C using Shimadzu UV-3600 and UV-3100PC spectrometers with a quartz cell having an optical length of 1 cm. XPS spectra were measured with a PHI 5000 VersaProbe (Ulvac-Phi, Inc.). Al Kα (15 kV, 25 W) radiation was used as the X-ray source. The beam was focused on a 100 μm^2 area. Samples were sputtered with an Ar ion gun to remove the oxidized surface prior to the measurements. The spectra were analyzed with the MultiPak software (Physical Electronics), and were standardized according to the Au $4f_{7/2}$ peak at 84.0 eV. Background subtract, peak smoothing and fitting were

used to estimate peak areas. STEM images were obtained using a transmission electron microscope (JEOL, ARM-200F) and the HAADF method. STEM samples were deposited on a super high-resolution carbon film with a Cu mesh (Okenshoji Co.). Cyclic voltammetry was performed using a BAS ALS750B analyzer. A glassy carbon disc electrode and platinum wire were used as the working and counter electrodes, respectively. An Ag^+/Ag (0.01 M $AgNO_3$ in 0.1 M Bu_4NClO_4/acetonitrile) electrode was used as the reference electrode. $NaPF_6$ (0.05 M) was used as the electrolyte.

Calculations. Geometry optimizations for Al_4, Al_{12}, Al_{13}, and Al_{28} in anionic and neutral states were carried out with the B3LYP/6–31 G(*d*, *p*) level of theory. The employed structures were based on the past literatures[34,35]. Vibrational analyses were also conducted for all the optimized structures and no imaginary frequency appeared. For the theoretical interpretation of the observed XPS data, Mulliken and natural population analyses were performed. In addition, the 2*p* orbital levels were calculated by single-point energy calculations with the GB3LYP/DZP-DKH level of theory within fourth-order Douglas–Kroll–Hess relativistic approximation, which is aimed at the incorporation of spin-orbit coupling. The diameter of Al_{13}^- was estimated using the Monte-Carlo method, in which the molecular volume was defined as the volume inside a contour with a density of 10^{-3} electrons/Bohr^3. All the calculations were conducted with Gaussian 16[44].

Data availability. The data that support the findings of this study are available from the corresponding author upon reasonable request.

Received: 16 February 2017 Accepted: 15 November 2017
Published online: 11 December 2017

References

1. Khanna, S. N. & Jena, P. Atomic clusters: building blocks for a class of solids. *Phys. Rev. B* **51**, 13705 (1995).
2. Reveles, J. U. et al. Designer magnetic superatoms. *Nat. Chem.* **1**, 310–315 (2009).
3. Yang, H. et al. Ligand-stabilized $Au_{13}Cu_x$ (x = 2, 4, 8) bimetallic nanoclusters: ligand engineering to control the exposure of metal sites. *J. Am. Chem. Soc.* **135**, 9568–9571 (2013).
4. Yang, H. et al. All-thiol-stabilized Ag_{44} and $Au_{12}Ag_{32}$ nanoparticles with single-crystal structures. *Nat. Commun.* **4**, 2422 (2013).
5. de Heer, W. A. The physics of simple metal clusters: experimental aspects and simple models. *Rev. Mod. Phys.* **65**, 611–676 (1993).
6. Li, X., Wu, H., Wang, X.-B. & Wang, L.-S. s-p Hybridization and electron shell structures in aluminum clusters: a photoelectron spectroscopy study. *Phys. Rev. Lett.* **81**, 1909–1912 (1998).
7. Bergeron, D. E., Castleman Jr, A. W., Morisato, T. & Khanna, S. N. Formation of $Al_{13}I^-$: evidence for the superhalogen character of Al_{13}. *Science* **304**, 84–87 (2004).
8. Reveles, J. U., Khanna, S. N., Roach, P. J. & Castleman, A. W. Jr. Multiple valence superatoms. *PNAS* **103**, 18405–18410 (2006).
9. Castleman, A. W. Jr. et al. From designer clusters to synthetic crystalline nanoassemblies. *Nano Lett.* **7**, 2734–2741 (2007).
10. Reber, A. C., Khanna, S. N. & Castleman, A. W. Jr. Superatom compounds, clusters, and assemblies: ultra alkali motifs and architectures. *J. Am. Chem. Soc.* **129**, 10189–10194 (2007).
11. Knight, W. D. et al. Electronic shell structure and abundances of sodium clusters. *Phys. Rev. Lett.* **52**, 2141–2143 (1984).
12. Castleman, A. W. Jr. & Khanna, S. N. Clusters, superatoms, and building blocks of new materials. *J. Phys. Chem. C* **113**, 2664–2675 (2009).
13. Dietz, T. G., Duncan, M. A., Powers, D. E. & Smalley, R. E. Laser production of supersonic metal cluster beams. *J. Chem. Phys.* **74**, 6511–6512 (1981).
14. Jarrold, M. F., Bower, J. E. & Kraus, J. S. Collision induced dissociation of metal cluster ions: Bare aluminum clusters, Al^+_n (*n* = 3–26). *J. Chem. Phys.* **86**, 3876–3885 (1987).
15. Iñiguez, M. P., Lopez, M. J., Alonso, J. A. & Soler, J. M. Electronic and atomic structure of Na, Mg, Al and Pb clusters. *Z. Phys. D* **11**, 163–174 (1989).
16. Ganteför, G., Gausa, M., Meiwes-Broer, K. H. & Lutz, H. O. Photoelectron spectroscopy of jet-cooled aluminium cluster anions. *Z. Phys. D* **9**, 253–261 (1988).
17. Leuchtner, R. E., Harms, A. C. & Castleman, A. W. Jr. Aluminum cluster reactions. *J. Chem. Phys.* **94**, 1093–1101 (1991).
18. Leuchtner, R. E., Harms, A. C. & Castleman, A. W. Jr. Thermal metal cluster anion reactions: behavior of aluminum clusters with oxygen. *J. Chem. Phys.* **91**, 2753–2754 (1989).
19. Watanabe, T., Koyasu, K. & Tsukuda, T. Density functional theory study on stabilization of the Al_{13} superatom by poly(vinylpyrrolidone). *J. Phys. Chem. C* **119**, 10904–10909 (2015).
20. Chen, J., Luo, Z. & Yao, J. Theoretical study of tetrahydrofuran-stabilized Al_{13} superatom cluster. *J. Phys. Chem. A.* **120**, 3950–3957 (2016).
21. Han, Y.-K. & Jung, J. Does the "superatom" exist in halogenated aluminum clusters? *J. Am. Chem. Soc.* **130**, 2–3 (2008).
22. Tomalia, D. A. et al. A new class of polymers: starburst-dendritic macromolecules. *Polym. J.* **17**, 117–132 (1985).
23. Astruc, D., Boisselier, E. & Ornelas, C. Dendrimers designed for functions: from physical, photophysical, and supramolecular properties to applications in sensing, catalysis, molecular electronics, photonics, and nanomedicine. *Chem. Rev.* **110**, 1857–1959 (2010).
24. Yamamoto, K. & Imaoka, T. Precision synthesis of subnanoparticles using dendrimers as a superatom synthesizer. *Acc. Chem. Res.* **47**, 1127–1136 (2014).
25. Yamamoto, K., Higuchi, M., Shiki, S., Tsuruta, M. & Chiba, H. Stepwise radial complexation of imine groups in phenylazomethine dendrimers. *Nature* **415**, 509–511 (2002).
26. Tomalia, D. A. & Khanna, S. N. A systematic framework and nanoperiodic concept for unifying nanoscience: hard/soft nanoelements, superatoms, meta-atoms, new emerging properties, periodic property patterns, and predictive Mendeleev-like nanoperiodic tables. *Chem. Rev.* **116**, 2705–2774 (2016).
27. Yamamoto, K. et al. Size-specific catalytic activity of platinum clusters enhances oxygen reduction reactions. *Nat. Chem.* **1**, 397–402 (2009).
28. Imaoka, T. et al. Magic number Pt_{13} and misshapen Pt_{12} clusters: which one is the better catalyst? *J. Am. Chem. Soc.* **135**, 13089–13095 (2013).
29. Imaoka, T., Kitazawa, H., Chun, W.-J. & Yamamoto, K. Finding the most catalytically active platinum clusters with low atomicity. *Angew Chem. Int. Ed.* **54**, 9810–9815 (2015).
30. Satoh, N., Nakashima, T., Kamikura, K. & Yamamoto, K. Quantum size effect in TiO_2 nanoparticles prepared by finely controlled metal assembly on dendrimer templates. *Nat. Nanotechnol.* **3**, 106–111 (2008).
31. Albrecht, K. et al. Polymerization of a divalent/tetravalent metal-storing atom-mimicking dendrimer. *Sci. Adv.* **2**, e1601414 (2016).
32. Takahashi, M. et al. Finely controlled multimetallic nanocluster catalysts for solvent-free aerobic oxidation of hydrocarbons. *Sci. Adv.* **3**, e1700101 (2017).
33. Tanuma, S., Powell, C. J. & Penn, D. R. Proposed formula for electron inelastic mean free paths based on calculations for 31materials. *Surf. Sci.* **192**, L849–L857 (1987).
34. Aguado, A. & López, J. M. Structures and stabilities of Al_n^+, Al_n, and Al_n^- (n = 13-34) clusters. *J. Chem. Phys.* **130**, 064704 (2009).
35. Drebov, N. & Ahlrichs, R. Structures of Al_n, its anions and cations up to n = 34: a theoretical investigation. *J. Chem. Phys.* **132**, 164703 (2010).
36. Giesbers, M., Marcelis, A. T. M. & Zuilhof, H. Simulation of XPS C1s spectra of organic monolayers by quantum chemical methods. *Langmuir* **29**, 4782–4788 (2013).
37. Koutecky, J. & Fantucci, P. Theoretical aspects of metal atom clusters. *Chem. Rev.* **86**, 539–587 (1986).
38. Chou, M. Y. & Cohen, M. L. Electronic shell structure in simple metal clusters. *Phys. Lett. A* **113**, 420–424 (1986).
39. Rao, B. K. & Jena, P. Evolution of the electronic structure and properties of neutral and charged aluminum clusters: a comprehensive analysis. *J. Chem. Phys.* **111**, 1890–1904 (1999).
40. Ko, Y. J. et al. Electronic structure and properties of isoelectronic magic clusters: $Al_{13}X$ (X = H, Au, Li, Na, K, Rb, Cs). *J. Chem. Phys.* **133**, 124308 (2010).
41. Otero, N., Alsenoy, C. V., Karamanis, P. & Pouchan, C. Electric response properties of neutral and charged $Al_{13}X$ (X = Li, Na, K) magic clusters. A comprehensive ab initio and density functional comparative study. *Comput. Theor. Chem.* **1021**, 114–123 (2013).
42. Enoki, O., Katoh, H. & Yamamoto, K. Synthesis and properties of a novelphenylazomethine dendrimer with a tetraphenylmethane core. *Org. Lett.* **8**, 569–571 (2006).
43. Kitazawa, H., Albrecht, K. & Yamamoto, K. Synthesis of a dendrimer reactor for clusters with a magic number. *Chem. Lett.* **41**, 828–830 (2012).
44. Frisch, M. J. et al. *Gaussian 16 Revision A.03* (Gaussian, Wallingford, CT, USA, 2016).

Acknowledgements

We thank N. Nakagawa for the assistance with titration of $AlCl_3$, and K. Albrecht and J. Kakinuma for synthesis of the pyDPAG4. This study was supported in part by a Grant-in-Aid for Young Scientists (B) (15K17829), for Scientific Research (C) (17K05804) and for Scientific Research (S) (15H05757) from the Japan Society for the Promotion of Science (JSPS), the ERATO program of the Japan Science and Technology (JST) Agency (JPMJER1503), and the cooperative research program of the Network Joint Research Center for Materials and Devices of Japan. We thank Suzukakedai Materials Analysis

Division, Technical Department, Tokyo Institute of Technology, for the STEM analysis. The XPS measurement was conducted at the Advanced Characterization Nanotechnology Platform of the University of Tokyo, supported by the "Nanotechnology Platform" of the Ministry of Education, Culture, Sports, Science and Technology (MEXT), Japan.

Author contributions

T.K. carried out the experiments except for theoretical calculations. N.H. conducted the calculations. T.K., N.H., T.I., and K.Y. wrote the manuscript. K.Y. supervised this work and project through discussing the concept with T.K.

Additional information

Supplementary Information accompanies this paper at https://doi.org/10.1038/s41467-017-02250-4.

Competing interests: The authors declare no competing financial interests.

Reprints and permission information is available online at http://npg.nature.com/reprintsandpermissions/

Publisher's note: Springer Nature remains neutral with regard to jurisdictional claims in published maps and institutional affiliations.